ceramics

MDPI

*Article*

# Microstructure, Mechanical and Thermal Properties of ZTA/$Al_2TiO_5$ Ceramic Composites

**A. M. Hassan [1], Hamada Elsayed [2,3,*], M. Awaad [3], A. M. Saleh [1] and S. M. Naga [3]**

[1] Materials Engineering Department, Faculty of Engineering, Zagazig University, Zagazig 44519, Egypt; ahmedsaleh.1993@yahoo.com (A.M.S.)
[2] Department of Industrial Engineering, Università Degli Studi di Padova, 35131 Padova, Italy
[3] Refractories Ceramics and Building Materials Department, National Research Centre, El-Bohous Str., Cairo 12622, Egypt
* Correspondence: hamada.elsayed@unipd.it

**Abstract:** Zirconia-toughened alumina (ZTA)/$Al_2TiO_5$ composites were prepared via a sol–gel route. The prepared samples were uniaxially pressed and pressurelessly sintered at 1650–1700 °C for 1 h. The microstructure, densification, and X-ray diffraction patterns of the sintered ZTA/$Al_2TiO_5$ composites were investigated, and their mechanical properties, thermal coefficient, and shock resistance were characterized. The addition of $Al_2TiO_5$ hindered the grain growth of the alumina particles and enhanced the relative density, Vickers hardness, and bending strength of the composites compared with pure ZTA samples. The fracture toughness was improved by 19% upon the addition of 40 wt% $Al_2TiO_5$. Moreover, increasing the $Al_2TiO_5$ content resulted in an improvement in the thermal shock resistance.

**Keywords:** ZTA; aluminum titanite; fracture toughness; thermal shock resistance



**Citation:** Hassan, A.M.; Elsayed, H.; Awaad, M.; Saleh, A.M.; Naga, S.M. Microstructure, Mechanical and Thermal Properties of ZTA/$Al_2TiO_5$ Ceramic Composites. *Ceramics* **2023**, *6*, 1977–1990. https://doi.org/10.3390/ceramics6040121

Academic Editor: Sergey Mjakin

Received: 8 August 2023
Revised: 25 September 2023
Accepted: 29 September 2023
Published: 4 October 2023



## 1. Introduction

Zirconia ($ZrO_2$)-toughened alumina (ZTA) ceramics are being intensively investigated due to their excellent mechanical and thermal properties, such as high strength, dimensional stability, high-temperature strength, hardness, wear resistance, and thermal resistivity [1–3], which render them suitable for various applications ranging from structural and mechanical to biomedical applications. Many research studies have been devoted to enhancing the properties of ZTA composites. Thus, approaches such as the modulation of sintering, oxide addition, and the development of alternative synthesis routes have been explored to improve the fracture toughness of ZTA composites [4]. In particular, the introduction of second additives has been demonstrated to reduce the sintering temperature, tailor the microstructure, and enhance the final mechanical and thermal properties of ZTA ceramics.

Many authors have addressed the effect of ceramic additives on the properties of ZTA composites [5–8]. It was suggested that the addition of optimum amounts of additives in addition to using suitable techniques in sintering ZTA ceramics, such as temperature and soaking time, have an essential influence on improving both the mechanical and thermal properties of ZTA composites by the enhancement of their microstructure and the formation of secondary phases. For instance, the addition of titanium oxide ($TiO_2$) promotes the sintering and grain growth of alumina ($Al_2O_3$) [9] due to the improvement in diffusivity that occurs as a result of the increasing concentration of $Al^{3+}$ vacancies generated by the substitution of $Al^{3+}$ with $Ti^{4+}$ [10,11].

Aluminum titanate ($Al_2TiO_5$) is a well-known refractory material that offers high thermal properties such as low heat conductivity, high thermal shock resistance, low thermal expansion, and appropriate refractoriness [12,13]. Therefore, it is a good candidate as the second phase in $Al_2O_3$ ceramics to enhance their properties for tribological purposes [14,15].

Aluminum titanate ($Al_2TiO_5$) possesses a high melting point (1860 °C), low thermal conductivity (0.9–1.5 $Wm^{-1}$ $K^{-1}$), low thermal expansion coefficient (8.6 × $10^{-6}$ $K^{-1}$), and high thermal shock resistance, which is conducive to improving the alumina composites' mechanical and thermal properties [16–19]. Moreover, the limited ability to form a $TiO_2$ solution enhances the densification of $Al_2O_3$ [20]. Borrell et al. [21] studied the addition of 40 vol.% aluminum titanate to alumina to prepare $Al_2TiO_5/Al_2O_3$ composites via an in-situ sintering reaction. They concluded that there is an excellent enhancement in the mechanical properties of the final composite (approximately 24 GPa, 424 MPa, and 5.4 MPa m1/2 for Vickers's hardness, bending strength, and fracture toughness, respectively) due to the homogenous and finer microstructure obtained. Meybodi et al. [22] prepared $Al_2O_3/Al_2TiO_5$ composites by reaction sintering of $Al_2O_3$ and $TiO_2$ nano powders. They investigated that high sintering temperatures improved the densification and hardness of the composite. On the other hand, Moritz and Aneziris [23] stated that the presence of $Al_2TiO_5$ in alumina-rich magnesium aluminate improves the thermal shock resistance of the formed composite as a result of the micro-cracked structure of $Al_2TiO_5$ ceramics obtained.

This study describes the investigation of the effect of the addition of Aluminum titanate ($Al_2TiO_5$) on the microstructure, mechanical, and thermal properties of $ZTA/Al_2TiO_5$ composites. The composite structure was investigated via X-ray diffraction (XRD) and scanning electron microscopy (SEM) analyses. Moreover, composite' properties such as densification parameters, the thermal expansion coefficient, shock resistance, fracture toughness, and bending strength were evaluated and interrelated.

## 2. Materials and Methods

### *2.1. Materials and Synthesis Methods*

Samples composed of Zirconia ($ZrO_2$)-toughened alumina composition (ZTA), where Zirconia was stabilized with 5 mol% yttrium oxide ($Y_2O_3$), were prepared using the following starting materials: $Al_2O_3$ (99.98% purity, provided by Almatis Gmbh, Ludwigshafen, Germany), zirconium (IV) n-butoxide, and yttrium nitrate (made of yttria ($Y_2O_3$) provided by Strem Chemicals, Newburyport, MA, USA). The synthesis of 5 mol% yttria ($Y_2O_3$)-partially stabilized $ZrO_2$ (PSZ) was conducted according to reported procedures [24]. Briefly, 5 mol% Yttria-partially stabilized zirconia (Y-PSZ) was developed through hydrolysis of zirconium (IV)-n-butoxide (ZR, Stream Chemicals USA) and with the addition of yttrium nitrate (after the dissolution of yttrium oxide ($Y_2O_3$) in nitric acid $HNO_3$). The formed gel was dried at 120 °C overnight, and then was calcined at 900 °C for 2h, using a heating rate of 5 °C, to remove all organic and nitrate materials. After calcination, the synthesized powders were grounded, at 300 rpm for 2 h, in a zirconia jar using a planetary ball mill, to obtain fine powder free of agglomerates. The zirconia ($ZrO_2$)-toughened alumina composition (ZTA) was made by mixing powders of 90 wt% $Al_2O_3$ and 10 wt% Y-PSZ.

Aluminum titanate ($Al_2TiO_5$, AT) was prepared from aluminum isopropoxide ($C_9H_{21}O_3Al$) and titanium (IV) n-butoxide ($C_{16}H_{36}O_4Ti$) following the procedure described by Naga et al. [25]. Aluminum tri-isopropoxide ($(C_3H_7O)_3$-Al, purity > 99%, Sigma-Aldrich, Darmstadt, Germany) was hydrolyzed in distilled water at a ratio of 1:10 (Al:$H_2O$), under vigorous stirring at 80 °C for 3 h. After that, a stable and homogeneous sol was attained upon the addition of nitric acid (2 mL) to produce (sol 1). In addition, the stoichiometric amount of titanium tetrabutoxide ($C_{16}H_{36}O_4Ti$, Strem Chemicals, Newburyport, MA, USA) was dissolved in absolute ethanol. Distilled water was then added dropwise to the mixture with a ratio of 1:20 (Ti:$H_2O$). The mixture was kept under vigorous stirring at room temperature. Also, Nitric acid was added to ensure the complete hydrolysis of the mixture and the formation of stable and transparent sol (sol 2). At the end, sol 2 was added dropwise to sol 1 under stirring until gelation occurred at 80 °C. The obtained gel was dried at 120 °C overnight and then was calcined in an electric oven for 2 h at 900 °C, with a heating and cooling rate of 5 °C/min. After that, the calcined $Al_2TiO_5$ powders were grounded using a planetary ball mill. The XRD analysis was performed to determine the phase assemblage of the prepared ceramics.

The targeted composites of Aluminum titanate and Zirconia ($ZrO_2$)-toughened alumina were also achieved by a mechanical mixing route. The batch compositions are given in Table 1. Cylindrical green ballets of ZTA/$Al_2TiO_5$, with dimensions of 13 mm in diameter and 4 mm in height, were obtained via uniaxial pressing at 240 MPa followed by pressureless sintering at different temperatures of 1650 °C, 1675 °C, and 1700 °C for a holding time of 1 h, with heating and cooling rates of 5 °C/min.

**Table 1.** Composition of AT/ZTA batches, wt%.

| Batch Symbol | Composition (wt%) | |
|---|---|---|
| | **ZTA** | **$Al_2TiO_5$** |
| Z0 | 100 | 0 |
| Z1 | 90 | 10 |
| Z2 | 80 | 20 |
| Z3 | 70 | 30 |
| Z4 | 60 | 40 |

### *2.2. Characterization*

The densification behavior of the obtained composite samples was investigated according to the liquid displacement method (ASTM C-20). The different crystal phases of the powdered samples developed after sintering were characterized by means of X-ray diffraction analysis (XRD) with a Philips X-ray diffractometer, model PW1730, with a Cu target and Ni filter. The XRD patterns were obtained at room temperature with a goniometric range of 10–70° 2θ.

The microstructure of the polished surfaces of the sintered specimens was examined with a scanning electron microscope (SEM-Jeol JSM-T20). The samples were thermally etched at 50 °C lower than the sintering temperature for 20 min in air and coated with gold (15 nm thickness) by means of electro-deposition in order to impart electric conduction.

### *2.3. Mechanical Testing*

Vickers hardness measurements were conducted using a hardness tester (Omnimet automatic MHK system Model Micro Met 5114, Buehler, Lake Bluff, IL, USA) according to the method described by Anstis et al. [26]. The bending strength was determined using a universal testing machine (Model LLOYD LRX5K of capacity 5 KN). Tested samples were polished to a mirror surface. The measurements were conducted under a crosshead speed of 0.5 mm/min and 25 mm support distance. Ten specimens were measured for each data point. The following equation is used to evaluate the bending strength from the fracture load obtained in the three-point bending test:

$$\sigma = 3P_fL/2wt^2$$

where $\sigma$ is the bending strength, $P_f$ is the fracture load, $L$ is the length of the specimen, $w$ is the specimen width, and $t$ is the thickness of the specimen $t$. The fracture toughness was measured using the single-edge v-notched beam (SEVNB) technique [27]. For the SEVNB method, ground and polished rectangular specimens ($3 \times 4 \times 45$ mm$^3$) were notched on the surface ($3 \times 45$ mm$^2$) using a diamond-charged cutting wheel, perpendicular to the length of the rectangular bars. The depth of the notches was approximately 0.7 mm, i.e., $\leq$20% of the height of the specimen in accordance with DIN 51109 [28]. The fracture toughness was determined by applying the following equation [29]:

$$K_{1c} = [L_{max}/t\,(h^{1/2})] \times [L_0 - L_i/h] \times [3R_M\,(d/h)^{1/2}/2(1 - d/h)^{3/2}]$$

where $L_{max}$ is the maximum load, $L_0$ and $L_i$ are the outer and inner roller spans, respectively, $t$ and $h$ are the thickness and height of the specimen, and $d$ is the depth of the sharpened notch.

$$R_M = [1.9887 - 1.326\,(d/h) - [3.49 - 0.68\,(d/h) + 1.35\,(d/h)^2]\,(d/h)\,(1 - (d/h)]/(1 + (d/h))^2.$$

### *2.4. Thermal Measurements*

Thermal expansion experiments were performed on triangle bars with dimensions of 25 mm × 5 mm × 5 mm, which were heated from ambient temperature up to 1100 °C at a rate of 5 °C/min for both heating and cooling processes employing a NETZSCH DIL 402 PC dilatometer. The thermal shock resistance was measured using specimen bars with dimensions of 60 mm × 6 mm × 6 mm. The bars were heated from room temperature to 1000 °C at a rate of 5 °C/min, followed by holding the top temperature for 30 min. The hot specimens were then immersed for 10 min in water at room temperature. The abovementioned cycle was repeated up to 5, 10, 15, and 20 times for five specimens to measure the retained bending strength, and the mean values were calculated.

## 3. Results

### *3.1. Phase Assemblage of the PSZ and $Al_2TiO_5$ Ceramics*

The XRD patterns of the obtained 5 mol% yttria ($Y_2O_3$)-partially stabilized $ZrO_2$ (PSZ) and Aluminum titanate ($Al_2TiO_5$) powders are shown in Figures 1a and 1b, respectively. Figure 1a confirms the synthesis of PSZ with pure Zirconia ($ZrO_2$) as the main crystalline phase' where t-$ZrO_2$ represents the principal obtained phase with 89% of the overall $ZrO_2$ phase. Figure 1b shows The X-ray diffraction (XRD) patterns of the $Al_2TiO_5$ ceramics synthesized via the sol–gel technique after calcination at 900 °C. The interpretation of XRD demonstrated the presence of $Al_2TiO_5$ as the main crystalline phase in addition to trace residues of alumina ($Al_2O_3$) and titania ($TiO_2$), as previously reported in [11]. The relatively lower calcination temperature was favored due to its role in the assemblage of the nearly pure phase. In addition, the lower calcination temperature enhanced the thermal stability by avoiding the decomposition of $Al_2TiO_5$ into $Al_2O_3$ and $TiO_2$ that occurs at high calcination temperatures [30,31].

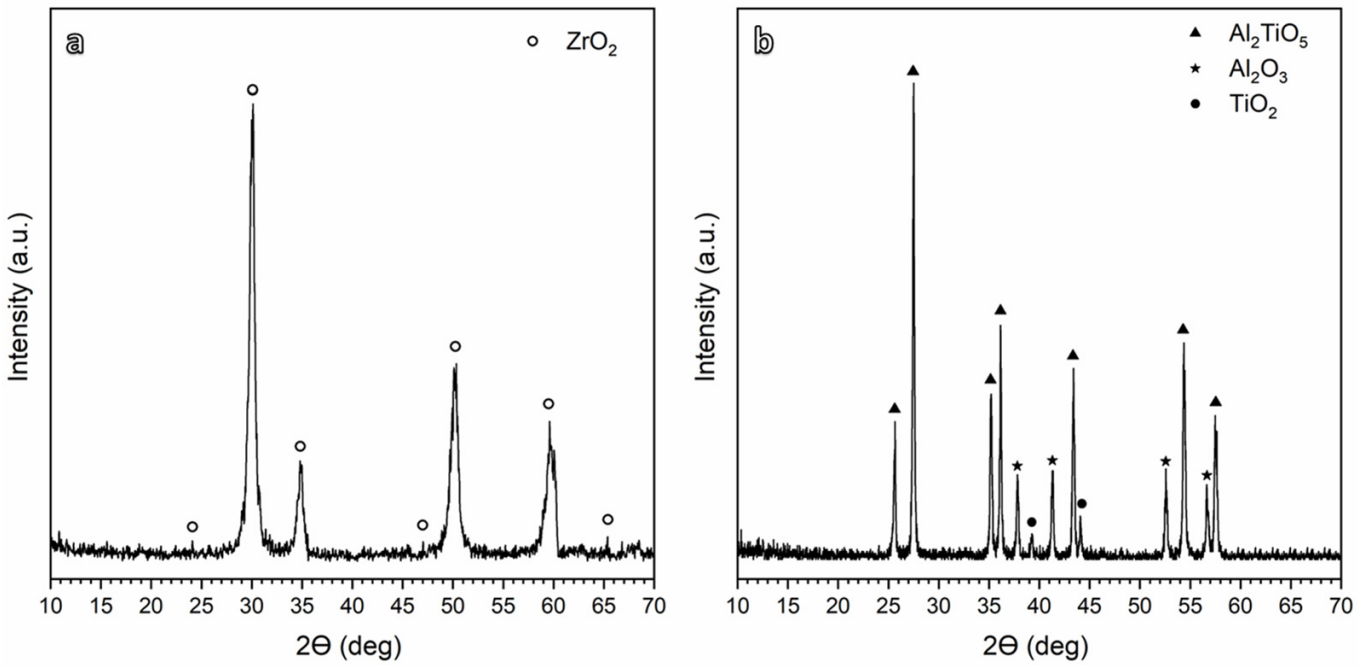


**Figure 1.** XRD patterns for (**a**) PSZ and (**b**) $Al_2TiO_5$ calcined at 900 °C.

### *3.2. Densification of the ZTA/$Al_2TiO_5$ Ceramic Composites*

Figure 2a,b shows the physical properties of the ZTA/$Al_2TiO_5$ composites as a function of the sintering temperature. Increasing the $Al_2TiO_5$ content from 10 to 40 wt% increased the bulk density of the studied samples when sintering at 1650 °C. Increasing the sintering temperature to 1700 °C and 1750 °C positively affected the bulk density of all samples. The apparent porosity showed the opposite trend, decreasing with both the $Al_2TiO_5$ content and the sintering temperature. This suggests that an alternative solid solution was created due to the presence of small $Ti^{4+}$ ions (0.064 nm) compared with the larger $Zr^{4+}$ ions (0.079 nm), which disrupted the crystalline structure, forming defects and enhancing the densification process [32].

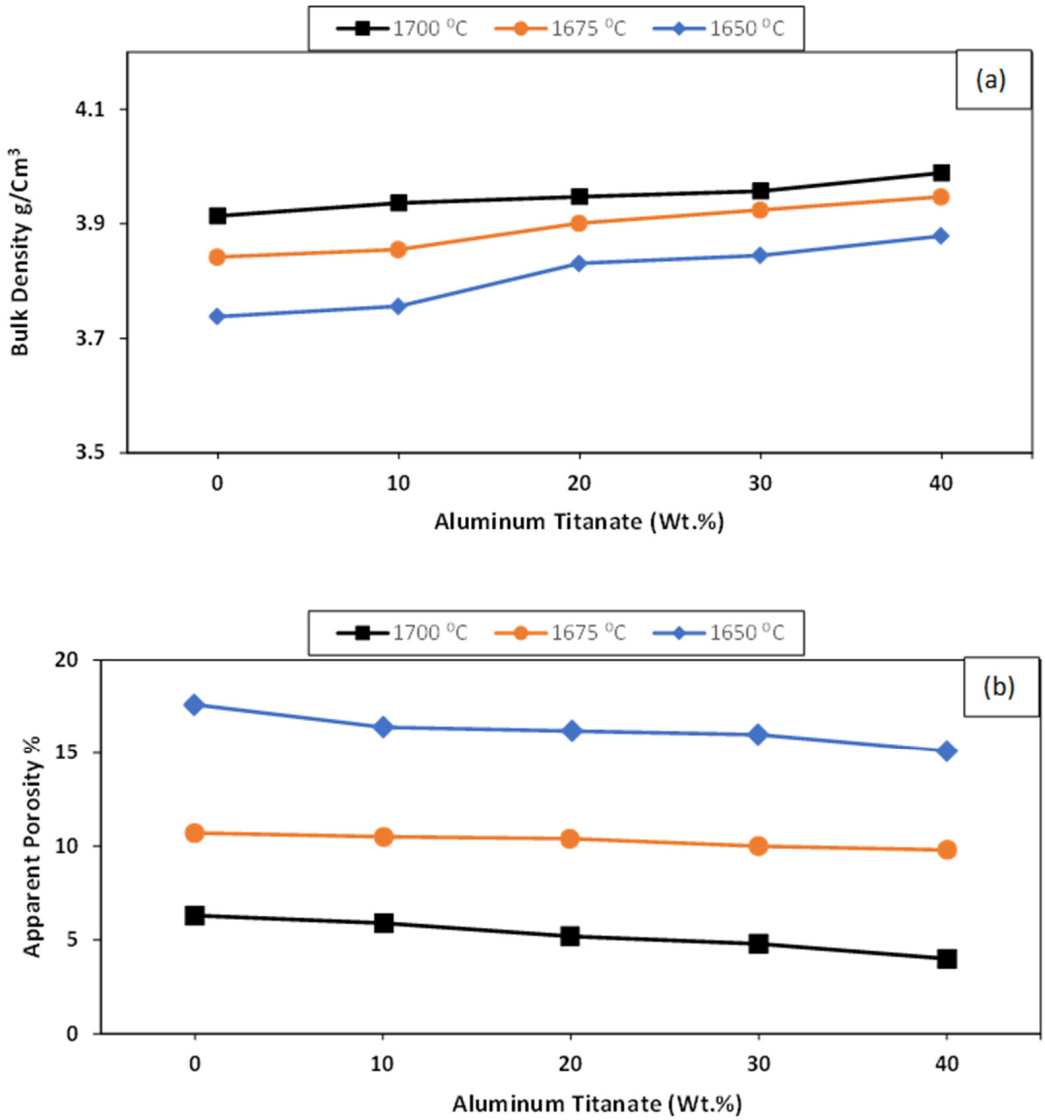


**Figure 2.** Densification parameters for AT/ZTA composites sintered at different sintering temperatures in terms of (**a**) bulk density g/$cm^3$ and (**b**) apparent porosity %.

Pure ZTA samples showed a low relative density of 93% when sintered at 1700 °C for 1 h (Figure 3), likely because of their poor sinterability stemming from the deficiency of defects in the $ZrO_2$ lattice [33]. In contrast, the addition of 40 wt% $Al_2TiO_5$ increased the relative density of the composites at the same sintering temperature. In general, ZTA/$Al_2TiO_5$ samples displayed higher relative density than pure ZTA samples.

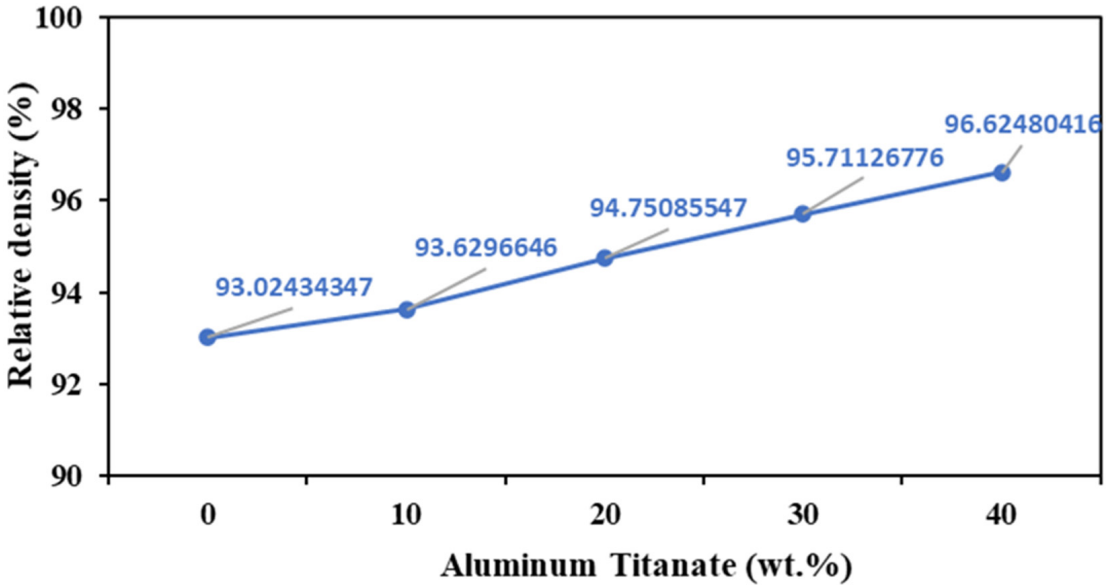


**Figure 3.** Relative density of AT/ZTA composites sintered at 1700 °C.

### *3.3. Phase Composition of the ZTA/$Al_2TiO_5$ Ceramic Composites*

The XRD diffraction patterns of the samples sintered at 1700 °C are shown in Figure 4, which revealed the presence of α-$Al_2O_3$, t-$ZrO_2$, and m-$ZrO_2$ as the main phase constituents and $Al_2TiO_5$ as a minor phase. The absence of any crystalline phases other than the starting phases proves that the sintered samples did not undergo dissociation even at the high sintering temperature of 1700 °C.

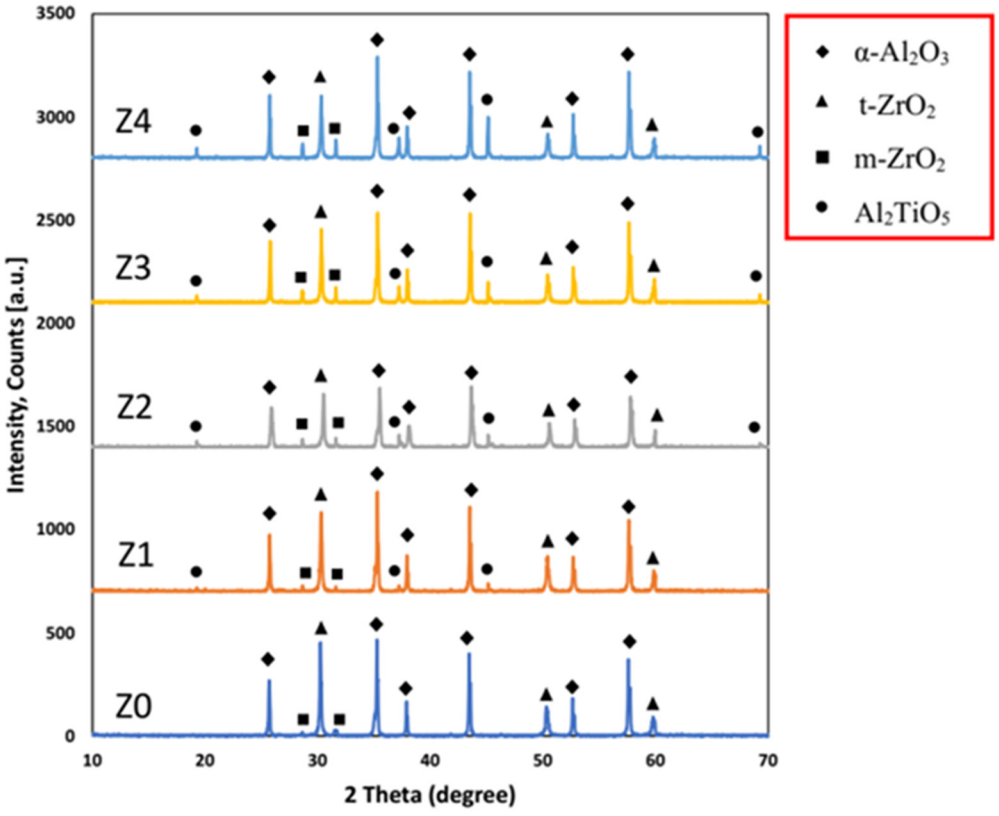


**Figure 4.** XRD diffraction pattern for the samples sintered at 1700 °C.

It was noticed that although the $ZrO_2$ content decreased gradually with the increase in the $Al_2TiO_5$ content, the t-$ZrO_2$ content was almost constant. It may be due to the $Ti^{4+}$ enhancement of t-$ZrO_2$ formation. It is well known that $Ti^{4+}$ ions are smaller than $Zr^{4+}$ ions. During the sintering process, some $Ti^{4+}$ is partially substituted in the $Zr^{4+}$ lattice, leading to the lattice distorting and enhancing t-$ZrO_2$ retention [34,35]. Additionally, the presence of $Al_2TiO_5$ reduced the particle size of $ZrO_2$ to be smaller than the critical size needed for the transformation from the t-$ZrO_2$ to m-$ZrO_2$ [36,37].

### *3.4. Microstructure of ZTA/$Al_2TiO_5$ Ceramic Composites*

Representative SEM micrographs of the ZTA/$Al_2TiO_5$ composites sintered for 1 h at various sintering temperatures are shown in Figure 5a–d. Large equiaxed $Al_2O_3$ grains were observed for the samples with the lowest $Al_2TiO_5$ content (Z1 having 10% $Al_2TiO_5$). Meanwhile, increasing the $Al_2TiO_5$ content resulted in smaller and more homogeneously distributed $Al_2O_3$ grains (Figure 5d). Observation of the sample microstructure revealed that the grain size increased with the $Al_2TiO_5$ content, leading to the anisotropy of the matrix structure [38]. Microcracks were observed on all samples, which may be due to the anisotropy of $Al_2TiO_5$. Microcrack formation and $Al_2TiO_5$ grain growth have been previously described as very prevalent phenomena in $Al_2TiO_5$ ceramic bodies and are responsible for the matrix structure anisotropy leading to the lowering of the thermal expansion of the resultant composites [38–41]. The difference in the thermal expansion coefficient of the components of the sample matrix, i.e., $Al_2TiO_5$, $ZrO_2$, and $Al_2O_3$, and the consequent stress could be a second factor promoting the formation of microcracks.

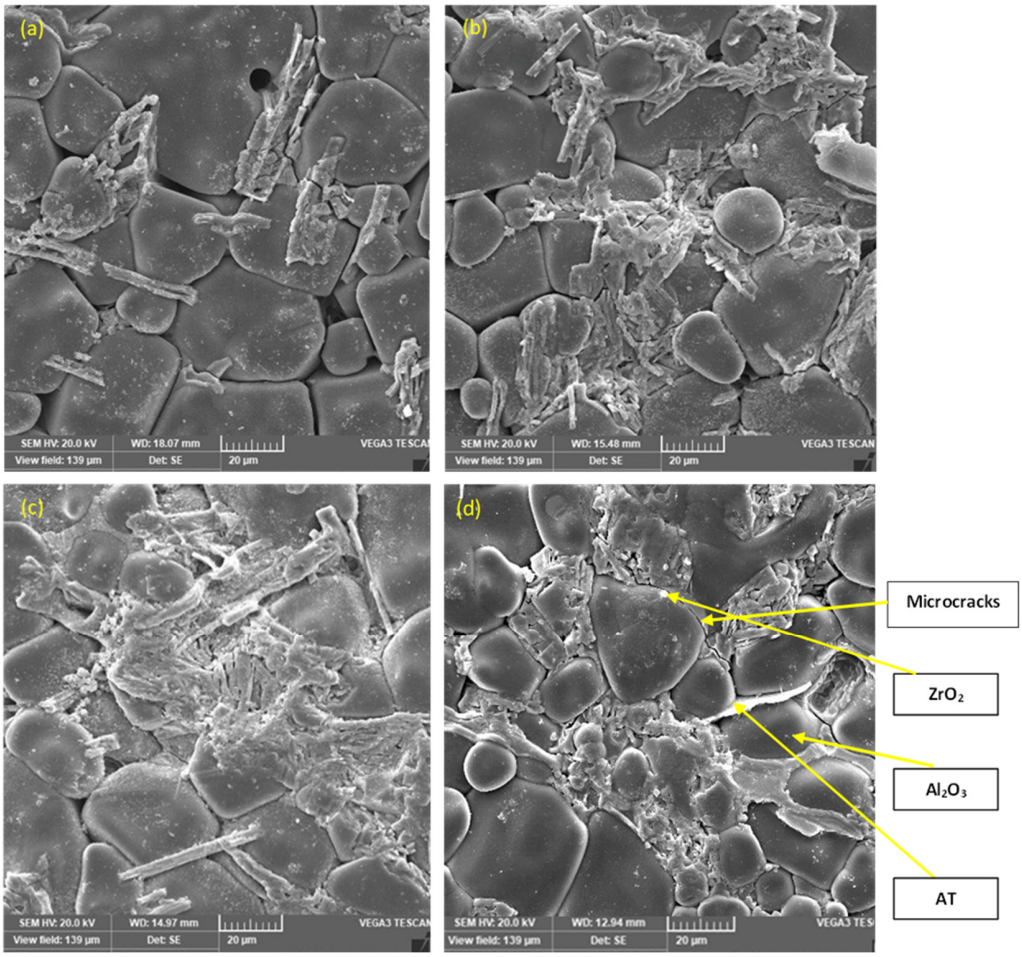


**Figure 5.** SEM micrographs of the polished, thermally etched sintered samples, (**a**) 10% AT, (**b**) 20% AT, (**c**) 30% AT, and (**d**) 40% AT.

When increasing the $Al_2TiO_5$ content, the $Al_2TiO_5$ crystals adopted an elongated morphology (rod-like shape). Figure 6a shows the microstructure of the Z4 sample (containing 40 wt% $Al_2TiO_5$), in which three types of $Al_2TiO_5$ crystals could be identified, namely, very fine crystals spattered all over the matrix, short rod-like crystals, and nonuniform crystals with no specific shape. An energy-dispersive X-ray spectroscopy analysis (Figure 6b) confirmed the formation of the three crystalline shapes of the $Al_2TiO_5$ phase.

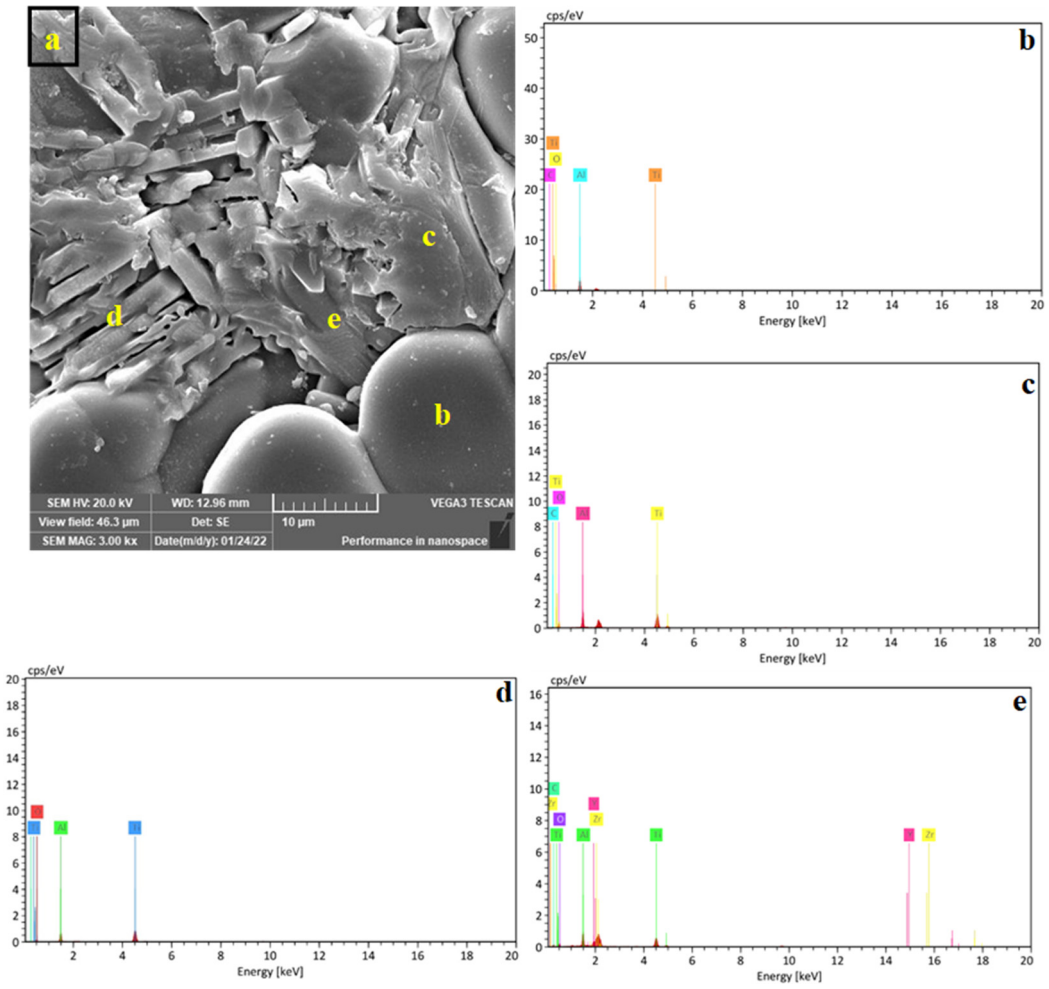


**Figure 6.** SEM micrograph of Z4 (40 mass % AT) sintered samples (**a**) and the EDS spectra (**b**–**e**) of the different AT shapes marked on subfigure (**a**).

### *3.5. Mechanical and Thermal Properties of the ZTA/$Al_2TiO_5$ Ceramic Composites*

The mechanical properties of the sintered samples, including bending strength, Vickers hardness, and fracture toughness, were determined as a function of the $Al_2TiO_5$ content.

#### 3.5.1. Three-Point Bending Strength Test Results

The addition of up to 20 wt% $Al_2TiO_5$ resulted in a steady increase in the bending resistance of the sintered bodies, as shown in Figure 7. While increasing the $Al_2TiO_5$ content to 30 wt% significantly increased the bending strength. The microstructure of bodies containing 30 wt% $Al_2TiO_5$ and the pore's shape and number reduction considerably enhanced the bending strength by lessening the loading area and thus enhanced the stress concentrations [42]. It is evident from Figure 2 that increasing the $Al_2TiO_5$ wt% reduced the porosity % from 6.3% to 4%. Less pronounced increases were observed upon further increasing the $Al_2TiO_5$ content to 40 wt%. This lower increase rate in the mechanical strength at $Al_2TiO_5$ content over 40 wt% can be attributed to the fact that $Al_2TiO_5$ became a major phase, and $Al_2O_3$ is known to be denser and have higher mechanical strength than

$Al_2TiO_5$. In addition, according to Ewais et al. [43], the difference in the thermal expansion coefficient between $Al_2O_3$ and $Al_2TiO_5$ is the main factor limiting the bending strength of the samples with higher $Al_2TiO_5$ content.

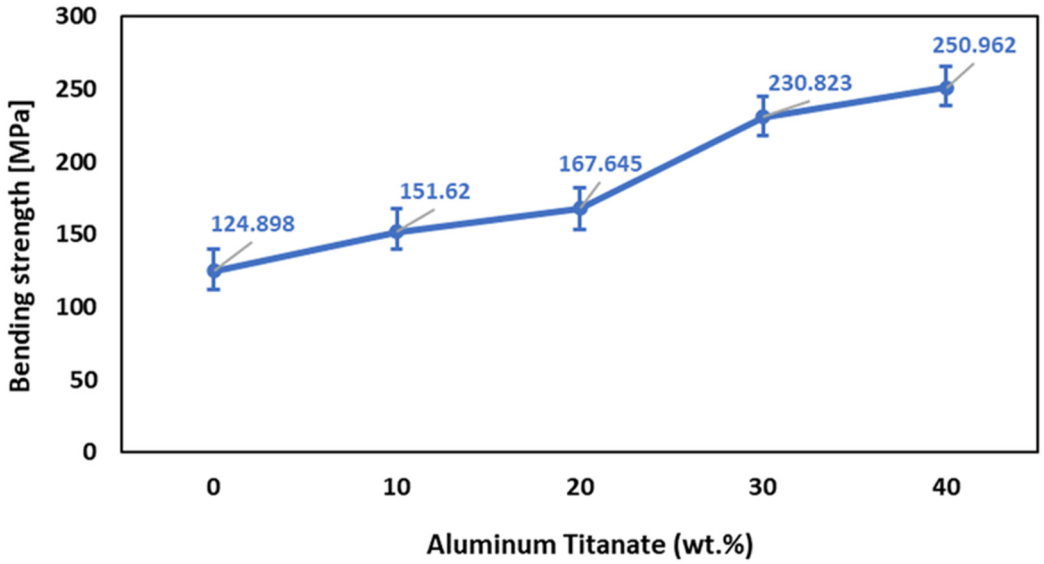


**Figure 7.** Effect of $Al_2TiO_5$ wt% content on the bending strength of AT/ZTA composite.

3.5.2. Vickers Hardness Measurements

The results of the Vickers hardness measurements for the sintered composite samples are illustrated in Figure 8, which shows that the increase in the $Al_2TiO_5$ content enhanced the Vickers hardness. The sintered samples containing 40 wt% $Al_2TiO_5$ displayed the highest hardness value (3652). Specifically, adding 40 wt% $Al_2TiO_5$ increased the hardness of the ZTA samples by 39%. The effect of the sintering behavior on the hardness must be taken into consideration. The improvement in the hardness with the increase in the $Al_2TiO_5$ content is due to the enhancement in the physical properties. Figure 5d shows the decrease in the porosity and the crack content in Z4 samples containing 40 wt% $Al_2TiO_5$, which also displayed the best hardness value, compared with other samples. Accordingly, it can be concluded that the hardness improved when improving the densification parameters of the samples, i.e., increasing the bulk density and decreasing the content of cracks and pores [9].

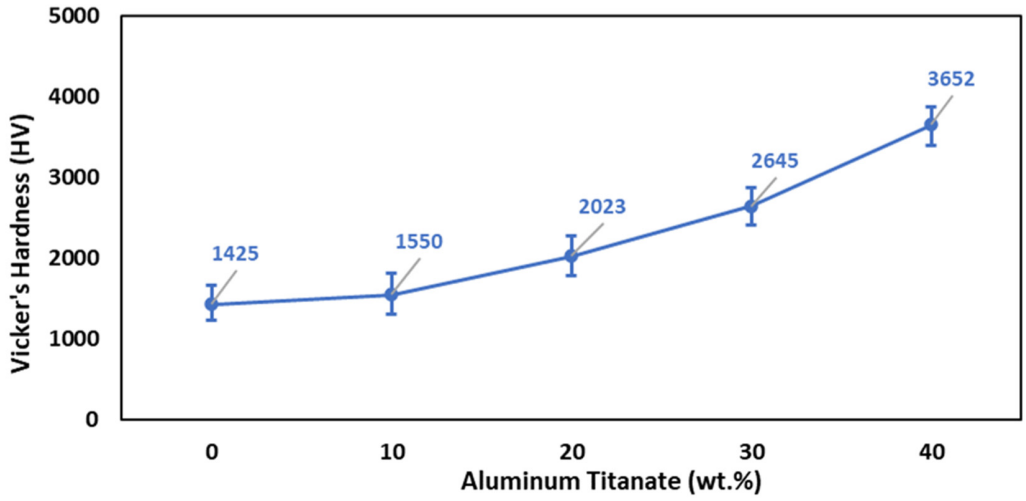


**Figure 8.** Effect of $Al_2TiO_5$ wt% content on the Vicker's hardness of AT/ZTA composite.

3.5.3. Fracture Toughness

The fracture toughness results shown in Figure 9 indicate that the addition of $Al_2TiO_5$ up to 20 wt% enhanced the fracture toughness. Specifically, the fracture toughness increased from 5.48 to 5.98 MPa $m^{1/2}$ when increasing the $Al_2TiO_5$ content from 0 and 20 wt%. Further addition of $Al_2TiO_5$ up to 40 wt% increased the fracture toughness by 19% (6.51 MPa $m^{1/2}$). The following factors can be invoked to explain the increase in the fracture toughness: (1) An increase in the content of $Al_2TiO_5$ rod-like grains, as shown in Figure 6, results in the movement of the cracks in many planes and around the grains composing the microstructure, crack bridging, which increases the energy required for fracture and boosts the fracture toughness [44,45]. At the same time, a transgranular fracture would need more energy in the presence of rod-like grains than with flat and plane grains. (2) Another factor is the presence of a secondary phase, $Al_2TiO_5$, which helps in increasing the fracture toughness through internal thermal effects [46–49]. With the increase in the $Al_2TiO_5$ content to 30 and 40 wt%, $ZrO_2$ could be partly dissolved in the $Al_2TiO_5$ phase, forming a thin grain boundary of an $Al_2O_3$–$TiO_2$–$ZrO_2$ amorphous solid solution. Such a grain boundary solid solution would promote grain boundary diffusion [50]. (3) Another factor is the decrease in the porosity content of the sintered bodies and the reduction in the alumina grain size with the increase in the $Al_2TiO_5$ content (Figures 2 and 5) also increases the fracture toughness. Porosity causes localized stresses at the grain boundaries, which weaken the intracrystalline binding and give rise to boundary looseness, enhancing the stress concentricity and the tendency to fracture [51].

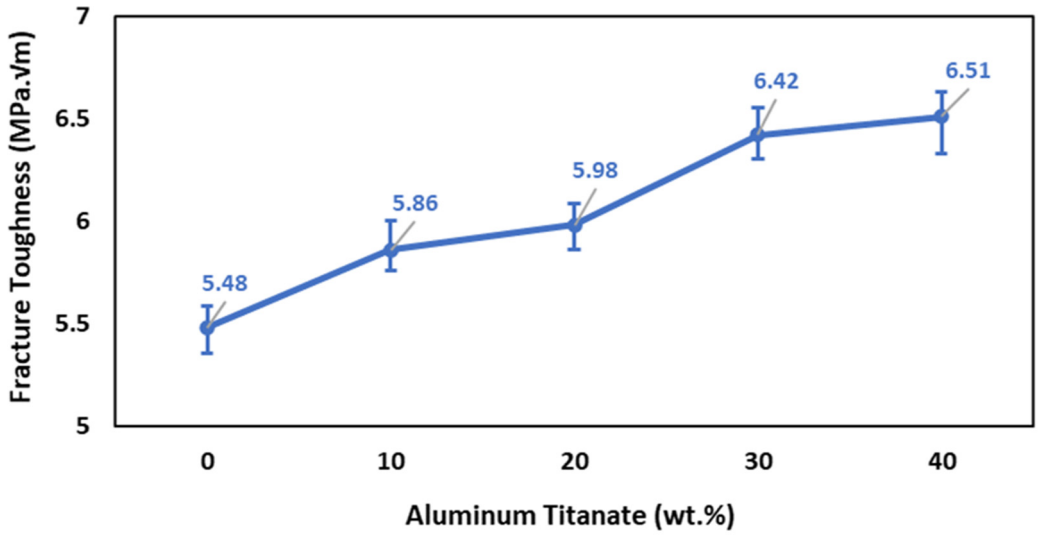


**Figure 9.** Effect of $Al_2TiO_5$ wt% content on the fracture toughness of AT/ZTA composite.

3.5.4. Reversible Thermal Expansion

$Al_2TiO_5$ exhibits a very low thermal expansion due to its large thermal expansion anisotropy [52]. In contrast, PSZ has a high thermal expansion because of the increase in its lattice constant with the addition of $Y_2O_3$, which decreases the lattice binding energy. Under normal conditions, the thermal expansion coefficient increases as the lattice constant increases [53] because the binding energy between cation and anion decreases with increasing the ionic distance. Furthermore, more oxygen vacancies in PSZ are formed by increasing the $Y_2O_3$ content, which decreases the binding energy of the crystal. Therefore, the thermal expansion coefficient of $ZrO_2$ becomes larger with the $Y_2O_3$ addition [54].

As expected, the thermal expansion coefficient decreases with the increase in the amount of aluminum titanate phase, which has a lower thermal expansion compared to both alumina and zirconia, according to the simple rule-of-mixtures for a two-phase composite, as shown in Figure 10. The previous results agree with the report by Zhu et al. [55], which deals with the addition of $TiO_2$ to $Nd_2O_3$–$Al_2O_3$–$SiO_2$ glass ceramics. In

addition, the increase in the crystal structure anisotropy of the samples containing higher $Al_2TiO_5$ content contributes to lowering the thermal expansion (Figure 5).

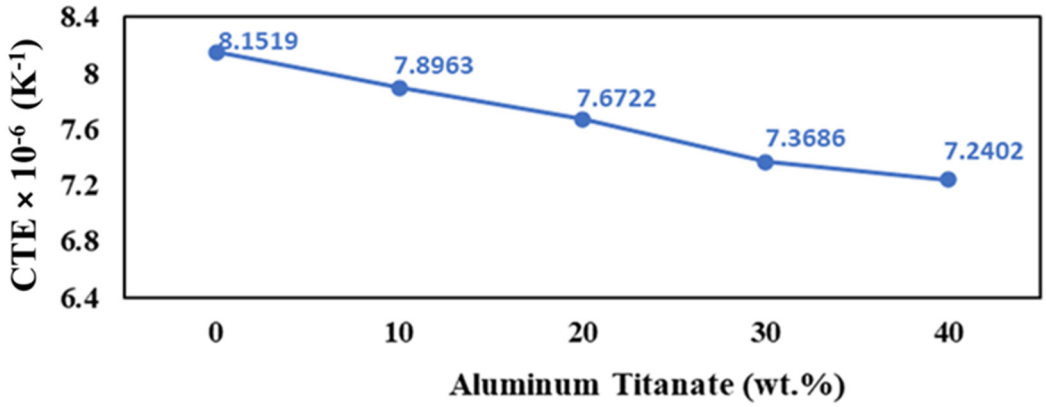


**Figure 10.** Thermal expansion of the AT/ZTA composites as a function of $Al_2TiO_5$ content.

3.5.5. Thermal Shock Resistance (TSR)

The TSR can be evaluated by measuring the bending strength after performing quenching experiments in water [56]. A three-point bending test was conducted after 5, 10, 15, and 20 cycles of TSR, and the results are shown in Figure 11.

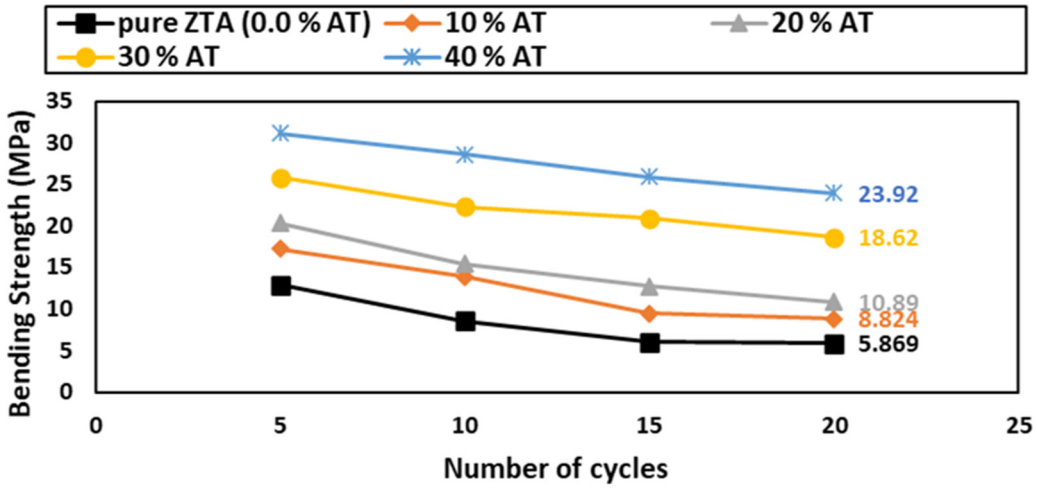


**Figure 11.** Reduction % in bending strength of AT/ZTA samples after 5, 10, 15, and 20 cycles of thermal shock.

After 20 thermal shock cycles, there was no sign of cracking or breakdown in any of the tested samples. The thermal shock of ceramic materials is affected by diverse factors, such as heat transmission, the sample form and size, and the mechanical and thermal properties and porosity % [57–59]. In general, ceramics are sentient to thermal shock because of their poor thermal conductivity properties. Consequently, sudden heat variations cause temporal thermal fatigue in ceramics, which results in either microcracking or even total failure [56].

Noteworthily, the TSR was improved by increasing the $Al_2TiO_5$ content. The $Al_2TiO_5$-free ZTA samples showed the worst results, which are in agreement with some researchers [59,60]. The TSR enhancement could be due to several factors, one of them being the pre-existing flaws in $Al_2TiO_5$ that enabled the flaw-tolerant during thermal shock. Also, it could be due to the mismatch in the thermal expansion coefficient of the constitutive phases, i.e., $8.2 \times 10^{-6}$ $K^{-1}$ for $\alpha$-$Al_2O_3$, $6.5 \times 10^{-6}$ $K^{-1}$ for m-$ZrO_2$, $10.5 \times 10^{-6}$ $K^{-1}$ for t-$ZrO_2$, and $1 \times 10^{-6}$ $K^{-1}$ for $Al_2TiO_5$. Such a mismatch can promote the formation of microcracks to some extent, which consumes stress energy and

prevents sample failure. In addition, these microcracks provide the transformation from t-$ZrO_2$ to m-$ZrO_2$ with sufficient space to occur, avoiding crack formation and sample failure [61,62]. Additionally, the microstructure toughening of the ZTA matrix containing $Al_2TiO_5$ particles as a second phase modulates the microstructure and enhances the TSR.

## 4. Conclusions

The following conclusions can be extracted from the investigation of the effect of $Al_2TiO_5$ addition on the microstructure, mechanical, and thermal properties of ZTA/$Al_2TiO_5$ composites:

(1) Three types of $Al_2TiO_5$ crystals were observed in the microstructure of the composites, i.e., very fine crystals spattered all over the matrix, short rod-like crystals, and nonuniform crystals with no specific shape, which affected the mechanical properties of the composites.

(2) The fracture toughness of the composites increased upon increasing the $Al_2TiO_5$ content up to 40% most likely due to an increase in the content of rod-like grains, which caused the displacement of cracks.

(3) The mismatch in the thermal expansion coefficient between the constitutive phases ($\alpha$-$Al_2O_3$, $ZrO_2$, and $Al_2TiO_5$) significantly enhanced the thermal shock resistance of the ZTA/$Al_2TiO_5$ composites compared with pure ZTA.

**Author Contributions:** Conceptualization, S.M.N. and M.A.; formal analysis, A.M.H. and H.E.; investigation, A.M.H., H.E., M.A., A.M.S. and S.M.N.; methodology, A.M.H. and A.M.S.; supervision, A.M.H. and S.M.N.; validation, A.M.H., H.E. and S.M.N.; writing—original draft, A.M.H., H.E. and A.M.S.; writing—review and editing, H.E. and S.M.N. All authors have read and agreed to the published version of the manuscript.

**Funding:** This research received no external funding.

**Institutional Review Board Statement:** Not applicable.

**Informed Consent Statement:** Not applicable.

**Data Availability Statement:** The data presented in this study are available upon request from the corresponding author.

**Conflicts of Interest:** The authors declare no conflict of interest. The funders had no role in the design of the study; in the collection, analyses, or interpretation of data; in the writing of the manuscript; or in the decision to publish the results.

## References

1. Sarker, S.; Mumu, H.T.; Al-Amin, M.; Alam, M.Z.; Gafur, M.A. Impacts of inclusion of additives on physical, microstructural, and mechanical properties of Alumina and Zirconia toughened alumina (ZTA) ceramic composite: A review. *Mater. Today Proc.* **2022**, *62*, 2892–2918. [CrossRef]
2. Dhar, S.A.; Mumu, H.T.; Sarker, S.; Bazlur Rashid, A.K.M. Influences of sintering time on the structures and mechanical properties of zirconia toughened alumina nanocomposites. *Mater. Today Proc.* **2021**, *44*, 1356–1360. [CrossRef]
3. Naga, S.M.; Awaad, M.; Bondioli, F.; Fino, P.; Hassan, A.M. Thermal diffusivity of ZTA composites with different YSZ quantity. *J. Alloys Compd.* **2017**, *695*, 1859–1862. [CrossRef]
4. Hofer, A.K.; Kraleva, I.; Prötsch, T.; Vratanar, A.; Wratschko, M.; Bermajo, R. Effect of second phase addition of zirconia on the mechanical response of textured alumina ceramics. *J. Eur. Ceram. Soc.* **2022**, *43*, 2935–2942. [CrossRef]
5. Tai, Q.; Mocellin, A. High temperature deformation of $Al_2O_3$-based ceramic particle or whisker composites. *Ceram. Int.* **1999**, *25*, 395–408. [CrossRef]
6. Bermejo, R.; Torres, Y.; Llanes, L. Loading configuration effects on the strength reliability of alumina–zirconia multilayered ceramics. *Compos. Sci. Technol.* **2008**, *68*, 244–250. [CrossRef]
7. Yang, Y.; Wang, Y.; Tian, W.; Wang, Z.Q.; Zhao, Y.; Wang, L.; Bian, H.M. Reinforcing and toughening alumina/titania ceramic composites with nano-dopants from nanostructured composite powders. *Mater. Sci. Eng. A* **2009**, *508*, 161–166. [CrossRef]
8. Fu, Y.; Gu, Y.W.; Du, H. SiC whisker toughened $Al_2O_3$-(Ti, W) C ceramic matrix composites. *Scr. Mater.* **2011**, *44*, 111–116. [CrossRef]
9. Manshor, H.; Aris, S.; Azhar, A.Z.A.; Abdullah, E.C.; Ahmad, Z.A. Effects of $TiO_2$ addition on the phase, mechanical properties, and microstructure of zirconia-toughened alumina ceramic composite. *Ceram. Int.* **2015**, *41*, 3961–3967. [CrossRef]

10. Wahsh, M.M.S.; Khattab, R.M.; Zawrah, M.F. Sintering and technological properties of alumina/zirconia/nano-$TiO^2$ ceramic composites. *Mater. Res. Bull.* **2013**, *48*, 1411–1414. [CrossRef]
11. Kalita, S.J.; Somani, V. $Al_2TiO_5$-$Al_2O_3$-$TiO_2$ nanocomposite: Structure, mechanical property and bioactivity studies. *Mater. Res. Bull.* **2010**, *45*, 1803–1810. [CrossRef]
12. Djambazov, S.; Lepkova, D.; Ivanov, I. A study of the stabilization of aluminium titanate. *J. Mater. Sci.* **1994**, *29*, 2521–2525. [CrossRef]
13. Buscaglia, V.; Nanni, P.; Battilana, G.; Aliprandi, G.; Carry, C. Reaction sintering of aluminium titanate: I effect of MgO addition. *J. Eur. Ceram. Soc.* **1994**, *13*, 411–417. [CrossRef]
14. Sobhani, M.; Ebadzadeh, T.; Rahimipour, M.R. Formation and densification behavior of reaction sintered alumina–20 wt.% aluminium titanate nano-composites. *Int. J. Refract. Met. Hard Mater.* **2014**, *47*, 49–53. [CrossRef]
15. Wang, X.T.; Padture, N.P.; Tanaka, H.; Ortiz, A.L. Wear-resistant ultra-fine-grained ceramics. *Acta Mater.* **2005**, *53*, 271–277. [CrossRef]
16. Runyan, J.L.; Bennison, S.J. Fabrication of flaw-tolerant aluminum-titanate reinforced alumina. *J. Eur. Ceram. Soc.* **1991**, *7*, 93–99. [CrossRef]
17. Lawn, B.R.; Padture, N.P.; Braun, L.M.; Bennison, S.J. Model for toughness curves in two phase ceramics: I, Basic fracture mechanics. *J. Am. Ceram. Soc.* **1993**, *76*, 2235–2240. [CrossRef]
18. Padture, N.P.; Runyan, J.L.; Bennison, S.J.; Braun, L.M.; Lawn, B.R. Model for toughness curves in two-phase ceramics: II. Microstructural variables. *J. Am. Ceram. Soc.* **1993**, *76*, 2241–2247. [CrossRef]
19. Ma, Q.; Shan, Q.; Chen, C.; Xu, Q.; Wang, Y.; Zhou, Y.; Shui, A. The influence of $ZrO_2$ on the microstructure and mechanical properties of $Al_2TiO_5$ flexible ceramics. *Mater. Charact.* **2022**, *185*, 111719–111728. [CrossRef]
20. Alves, P.C.F.; da Silva, D.G.; Vasconcelos, D.C.L.; Vilela, J.J.; Nascimento, J.F.; de Malo, D.C.; Vasconcelos, W.L. Microstructural characterization and mechanical properties on $Al_2O_3$–$TiO_2$ materials obtained by uniaxial pressing and extrusion. *Ceram. Int.* **2021**, *47*, 24988–24996. [CrossRef]
21. Borrell, A.; Salvador, M.D.; Rocha, V.G.; Fernández, A.; Molina, T.; Moreno, R. Enhanced properties of alumina-aluminium titanate composites obtained by spark plasma reaction-sintering of slip cast green bodies. *Compos. Part B* **2013**, *47*, 255–259. [CrossRef]
22. Meybodi, S.M.; Bafrooei, H.B.; Ebadzadeh, T.; Tazike, M. Microstructure and mechanical properties of $Al_2O_3$–20 wt% $Al_2TiO_5$ composite prepared from alumina and titania nanopowders. *Ceram. Int.* **2013**, *39*, 977–982. [CrossRef]
23. Moritz, K.; Aneziris, C.G. Enhancing the thermal shock resistance of alumina-rich magnesium aluminate spinel refractories by an aluminum titanate phase. *Ceram. Int.* **2016**, *42*, 14155–14160. [CrossRef]
24. Naga, S.M.; Abdelbary, E.M.; Awaad, M.; El-Shaer, Y.I.; Abd-Elwahab, H.S. Effect of the preparation route on the mechanical properties of Yttria–Ceria doped Tetragonal Zirconia/Alumina composites. *Ceram. Int.* **2013**, *39*, 1835–1840. [CrossRef]
25. Naga, S.M.; Awaad, M.; Saleh, A.M.; Hassan, A.M. Formation, Phase Stability, and Characterization of Unstabilized Aluminum Titanate ($Al_2TiO_5$) Ceramics. *Des. Eng.* **2021**, *9*, 17740–17754. [CrossRef]
26. Anstis, G.R.; Chantikul, P.; Lawn, B.R.; Marshall, B.D. A critical evaluation of indentation techniques for measuring fracture toughness: I, direct crack measurement. *J. Am. Ceram. Soc.* **1981**, *64*, 533–538. [CrossRef]
27. Tang, D.; Lim, H.; Lee, K.J.; Lee, C.; Cho, W. Evaluation of mechanical reliability of zirconia-toughened alumina composites for dental implants. *Ceram. Int.* **2012**, *38*, 2429–2436. [CrossRef]
28. *Prüfung von Keramischen Hochleistungswerkstoffen, Ermittlung der Risszähigkeit KIc (Testing High-Performance Ceramic Materials, Determination of the Fracture Toughness, KIc, in German)*; Beuth-Verlag: Berlin, Germany, 1991.
29. Munz, D.; Fett, T. *Ceramics: Mechanical Properties, Failure Behavior, Materials Selection*; Springer: Berlin, Germany, 1999.
30. Sathiyakumar, M.; Gnanam, F.D. Influence of MnO and $TiO_2$ additives on density, microstructure and mechanical properties of $Al_2O_3$. *Ceram. Int.* **2002**, *28*, 195–200. [CrossRef]
31. Keyvani, N.; Azarniya, A.; Hosseini, H.R.; Abeidi, M.; Moskovskikh, D. Thermal stability and strain sensitivity of nanostructured aluminum titanate ($Al_2TiO_5$). *Mater. Chem. Phys.* **2019**, *223*, 202–208. [CrossRef]
32. Azarniya, A.; Hosseini, H.R.; Amutha, C.; Ramakrishna, A. Effect of nanostructuring on thermal stability and decomposition of aluminium titanate ($Al_2TiO_5$): A phase transformation study. *Mater. Charact.* **2021**, *173*, 110764–110772. [CrossRef]
33. De Jonghe, L.C.; Rahaman, M.N. *Sintering of Ceramics, Handbook of Advanced Ceramics: Materials, Applications, Processing and Properties*; Elsevier Inc.: Amsterdam, The Netherlands, 2003; Volume 1–2, pp. 187–264.
34. Oishi, Y.; Ando, K.; Sakka, Y. Advances in Ceramics. *Am. Ceram. Soc.* **1983**, *7*, 208–219.
35. Hwang, C.S.; Chang, Y.J. Effects of $TiO_2$ on the microstructure and mechanical properties of $Al_2O_3/ZrO_2$ composites. *J. Mater. Res.* **1996**, *11*, 1545–1551. [CrossRef]
36. Clement, J.L.; Jarrett, P.S. Antibacterial silver. *Met. Based Drugs* **1994**, *1*, 467–482. [CrossRef] [PubMed]
37. Sotiropoulou, D.; Nikolopoulos, P. Work of adhesion in $ZrO_2$-liquid metal systems. *J. Mater. Sci.* **1993**, *28*, 356–360. [CrossRef]
38. Maki, R.S.; Suzuki, Y. Mechanical strength and electrical conductivity of reactively-sintered pseudobrookite-type $Al_2TiO_5$–$MgTi_2O_5$ solid solutions. *J. Ceram. Soc. Jpn.* **2016**, *124*, 1–6. [CrossRef]
39. Giordano, L.; Viviani, M.; Bottino, C.; Buscaglia, M.; Buscaglia, V.; Nanni, P. Microstructure and thermal expansion of $Al_2TiO_5$–$MgTi_2O_5$ solid solutions obtained by reaction sintering. *J. Eur. Ceram. Soc.* **2002**, *22*, 1811–1822. [CrossRef]

40. Ananthakumar, S.; Jayasankar, M.; Warrier, K. Microstructural, mechanical and thermal characterization of sol–gel-derived aluminium titanate–mullite ceramic composites. *Acta Mater.* **2006**, *54*, 2965–2973. [CrossRef]
41. Buessem, W.; Thielke, N.; Sarakauskas, R. Thermal expansion hysteresis of aluminum titanate. *Ceram. Age.* **1952**, *60*, 38–40.
42. Huang, Y.; Wu, D.; Zhao, D.; Niu, F.; Ma, G. Investigation of melt-growth alumina/aluminum titanate composite ceramics prepared by directed energy deposition. *Int. J. Extrem. Manuf.* **2021**, *3*, 035101–035116. [CrossRef]
43. Ewais, E.M.M.; Besisa, N.H.A.; Ahmed, A. Aluminum titanate based ceramics from aluminum sludge waste. *Ceram. Int.* **2017**, *43*, 10277–10287. [CrossRef]
44. Ahmad, I.; Islam, M.; Abdo, H.S.; Subhani, T.; Khalil, K.A.; Almajid, A.A.; Yazdani, B.; Zhu, Y.Q. Toughening mechanisms and mechanical properties of graphene nanosheet-reinforced alumina. *Mater. Des.* **2015**, *88*, 1234–1243. [CrossRef]
45. Chen, G.Q.; Zu, Y.F.; Luo, J.T.; Fu, X.S.; Zhou, W.L. Microstructure and superplastic behavior of $TiO_2$-doped $Al_2O_3$–$ZrO_2$ (3Y) composite ceramics. *Mater. Sci. Eng.* **2012**, *554*, 6–11. [CrossRef]
46. Yazdani, B.; Xia, Y.D.; Ahmad, I.; Zhu, Y.Q. Graphene and carbon nanotube (GNT)-reinforced alumina nanocomposites. *J. Eur. Ceram. Soc.* **2015**, *35*, 179–186. [CrossRef]
47. Yin, Y.; Ma, B.Y.; Hu, C.B.; Liu, G.Q.; Li, H.X.; Su, C.; Ren, X.M.; Yu, J.Y.; Zhang, Y.R.; Yu, J.K. Preparation and properties of porous SiC-$Al_2O_3$ ceramics using coal ash. *Int. J. Appl. Ceram. Technol.* **2019**, *16*, 23–31. [CrossRef]
48. Liu, Z.L.; Deng, C.J.; Yu, C.; Wang, X.; Ding, J.; Zhu, H.X. Molten salt synthesis and characterization of SiC whiskers containing coating on graphite for application in $Al_2O_3$-SiC-C castables. *J. Alloys Compd.* **2019**, *777*, 26–33. [CrossRef]
49. Tan, P.; Wu, P.; Gao, L.; Sui, Y.D.; Jiang, Y.H. Influence of $Si_3N_4$ content on the physical and mechanical properties of zirconia-toughened alumina (ZTA) ceramic composites. *Mater. Res. Express* **2019**, *6*, 065205. [CrossRef]
50. Fu, L.P.; Gu, H.Z.; Huang, A.; Ni, H.W. Correlations among processing parameters and porosity of a lightweight alumina. *Ceram. Int.* **2018**, *44*, 14076–14081. [CrossRef]
51. Fu, R.D.L.; Gu, H.; Huang, A.; Yang, S.; Chen, D. Effect of zirconia sol on the microstructure and properties of $Al_2O_3$-based ceramic fabricated from natural bauxite. *Ceram. Int.* **2022**, *48*, 12954–12961. [CrossRef]
52. Morsin, B.; Lynch, R.W. Structure studies on $Al_2TiO_5$ at room temperature and at 600 °C. *Acta Crystallogr. B* **1972**, *28*, 1040–1046. [CrossRef]
53. Touloukian, Y.S.; Kirby, R.K.; Taylor, R.E.; Lee, T.Y.R. Thermophysical Properties of Matter. In *Thermal Expansion Nonmetallic Solids*; Touloukian, Y.S., Ho, C.Y., Eds.; Plenum: New York, NY, USA, 1977; Volume 13.
54. Hayashi, H.; Saitou, T.; Maruyama, N.; Inaba, H.; Kawamura, K.; Mori, M. Thermal expansion coefficient of yttria stabilized zirconia for various yttria contents. *Solid State Ion.* **2005**, *176*, 613–619. [CrossRef]
55. Zhu, W.; Zhou, L.; Tang, M.; Zou, H.; Han, Y.; Ran, X. Effect of $TiO_2$ on the crystallization, thermal expansion and wetting behavior of $Nd_2O_3$-Al2$O_3$-$SiO_2$ glass ceramic filler. *J. Eur. Ceram. Soc.* **2021**, *41*, 351–357. [CrossRef]
56. Fantozzi, G.; Saâdaoui, M. Toughness, fatigue and thermal shock of ceramics: Microstructural effects. *Compr. Hard Mater.* **2014**, *2*, 299–319. [CrossRef]
57. Becher, P.F.; Alexander, K.B.; Bleier, A.; Waters, S.B.; Warwick, W.H. Influence of $ZrO_2$ grain size and content on the transformation response in the $Al_2O_3$—$ZrO_2$ (12 mol% $CeO_2$) System. *J. Am. Ceram. Soc.* **1993**, *76*, 657–663. [CrossRef]
58. Pettersson, P.; Johnsson, M.; Shen, Z. Parameters for measuring the thermal shock of ceramic materials with an indentation-quench method. *J. Eur. Ceram. Soc.* **2002**, *22*, 1883–1889. [CrossRef]
59. Shen, L.; Liu, M.; Liu, X.; Li, B. Thermal shock resistance of the porous $Al_2O_3/ZrO_2$ ceramics prepared by gelcasting. *Mater. Res. Bull.* **2007**, *42*, 2048–2056. [CrossRef]
60. Yu, R.; Zhang, L.; Zhang, X.; Liu, P.; Qi, H.; Wang, J.; Liu, X. Fracture behavior and thermal shock resistance of alumina-spinel castables-Effect of added fused zirconia-alumina. *Ceram. Int.* **2020**, *46*, 20732–20741. [CrossRef]
61. Wahsh, M.; Khattab, R.; Awaad, M. Thermo-mechanical properties of mullite/zirconia reinforced alumina ceramic composites. *Mat. Des.* **2012**, *41*, 31–36. [CrossRef]
62. Low, I.M.; Oo, Z. Reformation of phase composition in decomposed aluminium titanate. *Mater. Chem. Phys.* **2008**, *111*, 9–12. [CrossRef]